pISSN 1229-3008 eISSN 2287-6251
Progress in Superconductivity and Cryogenics
Vol.20, No.1, (2018), pp.1~10 https://doi.org/10.9714/psac.2018.20.1.001

Design of flux pinning property in REBCO coated conductors with artificial pinning centers

Teruo Matsushita*, and Masaru Kiuchi

Department of Computer Science and Electronics
Kyushu Institute of Technology, Iizuka, Japan

(Received 21 February 2018; revised or reviewed 3 March 2018; accepted 4 March 2018)

Abstract

The improvement of critical current properties of $REBa_2Cu_3O_{7-x}$ (REBCO) coated conductors by introducing artificial pinning centers (APCs) is examined with respect to the field-angle anisotropy, high-field performance and relaxation property with time. Nano-rods along the c-axis introduced by PLD method and isotropic nano-particles introduced by TFA-MOD method are treated.

The theoretical analysis is also shown to understand the effect of APCs quantitatively. The effects of superconducting layer thickness that influences the high-field performance and relaxation property are also discussed. It is shown that the upper critical field, which is another important factor to determine the high-field property, can be improved by introduction of APCs through electron scattering at interfaces with the superconducting matrix. The optimum critical current property can be obtained by properly designing the morphology and number density of APCs and the superconducting layer thickness.

Keywords : REBCO coated conductor, artificial pinning center, nano-rods, nano-particles, anisotropy, relaxation, layer thickness

1. INTRODUCTION

The critical current density (J_c) of REBCO coated conductors by natural pinning centers is not sufficiently high at 77.3 K and it suffers from strong anisotropy with respect to the direction of the magnetic field caused by the anisotropy of electron effective mass. That is, J_c is very high within a narrow range of the magnetic field angle around the a-b plane and is low over a relatively wide angle around the c-axis. Many trials have been made to improve the J_c property by introducing artificial pinning centers (APCs). The trend effective to improvement is roughly classified into two categories: One is nano-rods grown along the c-axis that directly improve the poor J_c in the field along this direction [1-6] and the other is isotopic nano-particles that indirectly improve by reducing the anisotropy in J_c by adding strong isotropic pinning forces [7-10]. Trails to improve J_c at low temperatures and at high magnetic fields are also examined for specific applications of high temperature superconductivity [11].

Introduction of APCs is also useful to enhance the irreversibility field and to suppress the effect of thermal activation of flux lines that influences seriously the stability of magnetic field produced by superconducting magnets as will be shown later. The important thing is to design APCs that are useful to improve the J_c property under desired condition of temperature and magnetic field for each application. For this purpose it is necessary to predict J_c exactly. Especially we need two theoretical treatments: one is the summation theory to predict J_c or the pinning force density (F_p) as a function of elementary pinning force (f_p) and number density (N_p) of pinning centers and the other is the flux creep and flow model [12] to estimate under the influence of flux creep. The elementary pinning force is the maximum force that one pinning center can exert. This makes us possible to design optimum APCs for the aimed application.

The summation problem was examined first by Labusch with a statistical method [13]. It predicted that the contribution of one pinning center to the pinning force density, F_p/N_p, is proportional to f_p^2, which is called the statistical summation property, for f_p sufficiently higher than the threshold value, f_{pt}, and is zero for f_p below f_{pt}. Experiments clarified later that F_p/N_p was proportional to f_p and f_p^2, for strong and weak pinning centers, respectively, as shown in Fig. 1 [14]. The first property is called the linear summation. The statistical summation property was found to hold down to very weak pinning centers with f_p smaller by a factor of 10^{-4} than f_{pt}. Later Campbell [15] proposed a new theoretical model in which the variation in the pinning force of each pinning center was assumed to be periodic with respect to the displacement of flux lines. This was successful to explain that F_p approaches the linear summation when f_p is sufficiently large. However, the problem of the threshold value remained.

In 1979 Larkin and Ovchinnikov [16] proposed their theoretical model and attributed the non-zero threshold value in the Labusch theory to the assumption of the long range order of flux line lattice that does not exist because of finite pinning correlation lengths. In addition, the

* Corresponding author : matsushita.teruo391@mail.kyutech.ac.jp

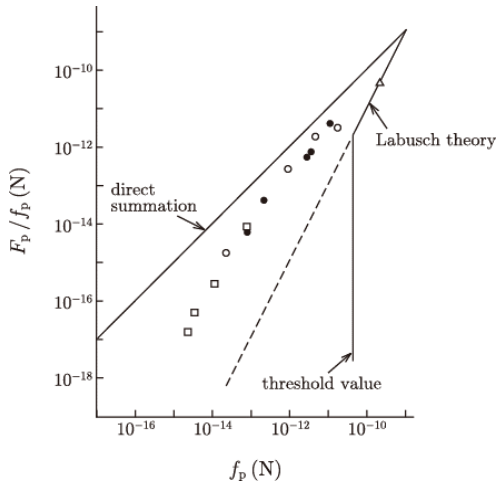

Fig. 1. Contribution to the pinning force density from one pinning center (F_p/N_p) vs. the elementary pinning force (f_p) for Nb at 4.2 K and at the reduced magnetic field of $B/B_{c2} = 0.55$ [14].

problematic point in the Labusch theory was that it was not a self-consistent mean field theory [17]. That is, although the Labusch parameter (α_L) was introduced as a mean-field parameter that represents the strength of the flux pinning, it was treated to be independent of F_p. The coherent potential approximation theory [18] was proposed based on these points and it explained the experimental results in [14]. The obtained threshold value itself was a function of f_p and was always smaller than f_p. Hence, it explains that even a very weak pinning center contributes with its own strength to the pinning force density. At the same time it was shown that the predicted pinning force density in the linear summation regime agreed quantitatively with experiments for the pinning by normal precipitates [19]. It should be noted that the fact that f_p is larger than f_{pt} proves that the pinning loss has a nature of hysteresis loss independent of the viscous coefficient, although the loss mechanism itself is viscosity [20].

The above theoretical investigation has clarified that the pinning obeys the linear summation for artificially introduced strong pinning centers. Fortunately this makes the theoretical analysis easy. However, the serious problem we have is that the pinning by small natural defects such as oxygen deficiencies has an appreciable contribution and we have no information on f_p and N_p for these defects. What we can do is to estimate its contribution from measurement of samples with no artificial pinning centers. In this case it will be allowed to assume the collective summation for the resultant pinning force density because of no spatial correlation between natural defects and artificially introduced pinning centers:

$$F_p = \left({F_{np}}^2 + {F_{ap}}^2\right)^{1/2}, \quad (1)$$

where F_{np} and F_{ap} are the pinning force densities of natural and artificial pinning centers, respectively.

Another factor that exists between the theoretical estimation of the summation theory and practical critical current density is the thermal activation of pinned flux lines. The theoretical approach to estimate the practical critical current density from the virtual flux creep-free pinning force density is briefly described in Appendix.

In this paper we treat the improvements of field-angle anisotropy, irreversibility field and relaxation rate by introduction of APCs. It should be noted that the thickness of superconducting layer is another important factor that influences the flux creep property [21]. Hence, the effect of superconducting layer thickness is also discussed.

2. IMPROVEMENT OF PINNING CHARACTERISTICS BY APCs

2.1. Field-angle anisotropy

Here we show examples of improvement of the field-angle anisotropy by introducing APCs. Figure 2 shows the improvement by introduction of $BaZrO_3$ (BZO) nanorods to $GdBa_2Cu_3O_{7-x}$ coated conductor [22]. The samples were deposited using PLD technique on IBAD substrates and the superconducting layer thickness was 2.28 μm. The diameter and length of the nono-rods were about 5 nm and 60 nm, respectively. It is found that the field angle anisotropy is very weak without a pronounced peak in the magnetic field along the c-axis for the sample with the BZO nano-rods. This is ascribed to widely distributed growth direction of the nano-rods around the c-axis shown in Fig. 3, where φ is the declination angle from this axis. This distribution is associated with the structure of nono-rods called "fireworks" that is sometimes observed in $YBa_2Cu_3O_{7-x}$ coated conductors with BZO nano-rods. Another point is disappearance of sharp peak at around $\theta = 90°$. This can be explained by the mechanism of collective pinning shown by Eq. (1): It is considered that the pinning force of nano-rods F_{ap} is much stronger than that of stacking faults F_{np} because of a large difference in the interaction volume (the volume of overlapping region between the vortex core and pinning center). Then, Eq. (1) leads to

$$F_p \cong F_{ap} + \frac{{F_{np}}^2}{2F_{ap}}. \quad (2)$$

Thus, the contribution of stacking faults given by the second term is very small and the disappearance of the peak in the in-plane field can be explained even if the stacking faults are not appreciably changed by introducing nano-rods. It is considered that development of fabrication process that realizes nano-rods with a wide distribution of the growth direction is important.

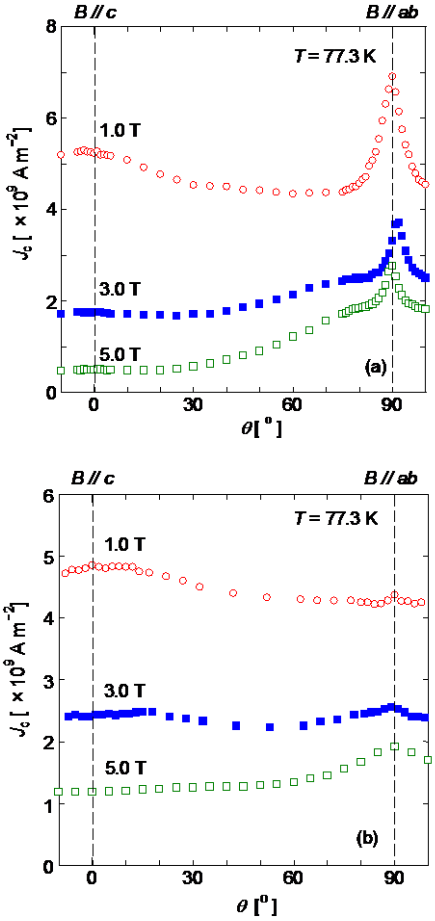

Fig. 2. Field angle anisotropy of critical current density in $GdBa_2Cu_3O_{7-x}$ coated conductor (a) without and (b) with $BaZrO_3$ nano-rods [22].

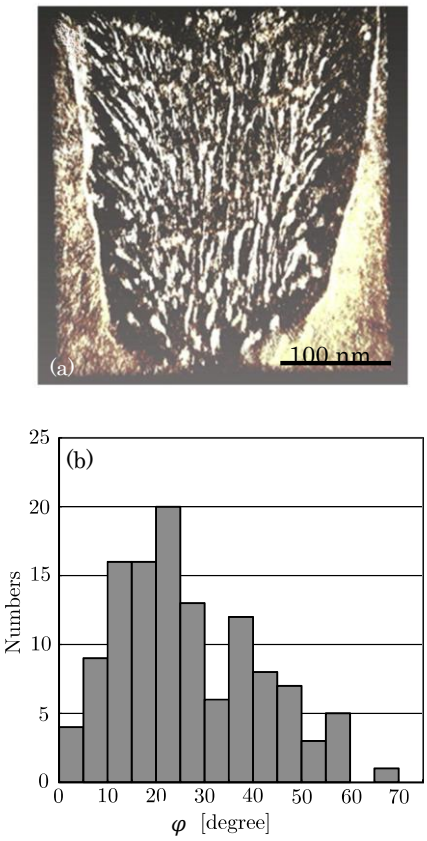

Fig. 3. (a) Three dimensional structure of nan-rods obtained by transmission electron microscopy and electron tomography and (b) distribution of angle of growing direction of $BaZrO_3$ nano-rods measured from the c-axis in $GdBa_2Cu_3O_{7-x}$ coated conductor [22].

Figure 4 shows the field-angle dependent J_c of TFA-MOD processed (YGa)$Ba_2Cu_3O_{7-x}$ (YGdBCO) coated conductor with and without BZO nano-particles [23]. The superconducting layer thickness was about 0.5 μm for the both samples and the critical temperature was 90.0 and 90.2 K for the samples without and with nano-particles, respectively. The mean diameter of nano-particles was about 20 nm. The J_c increases over a wide range of the field-angle except at around the in-plane field direction, resulting in a reduction in the anisotropy. Thus, proper introduction of APCs enables to achieve more isotropic J_c. Hence, the design of pinning morphology is very important for the purpose.

2.2. High field property

Figure 5 shows an example of the improvement of J_c determined by magnetization measurement at 77.3 K in the magnetic field along the c-axis by introduction of BZO and $BaHfO_3$ (BHO) nano-rods to PLD processed $GdBa_2Cu_3O_{7-x}$ coated conductor with the superconducting layer of about 1 μm thick [24]. The added amount of BZO and BHO to form nano-rods was 3.5 mol% and the resultant volume fraction of nano-rods was about 1.5 % for the both cases. The specification of the samples is given in Table 1. BHO nano-rods were slightly thinner. Although J_c at low magnetic field does not change appreciably, the high-field J_c is dramatically improved, resulting in the enhanced irreversibility field.

2.3. Relaxation property

Figure 6 shows the magnetic J_c at 20 K in the magnetic field along the c-axis for the samples shown in Fig. 4. The trend is similar to the result in Fig. 5 and the improvement is better for the sample with BHO nano-rods. The magnetic relaxation is measured from about 1 min. to 1 h after starting the measurement and the observed magnetization normalized by the initial value is plotted versus the

TABLE I
SPECIFICATION OF PLD PROCESSED $GdBa_2Cu_3O_{7-x}$ SAMPLES [24].

Sample	Material	Amount of addition (mol%)	Thickness d (μm)	T_c (K)	Mean diameter of nano-rods (nm)
Pure	GdBCO	--	1.1	90.7	--
BHO	GdBCO+BHO	3.5	1.0	90.5	4.5
BZO	GdBCO+BZO	3.5	1.1	89.2	5.6

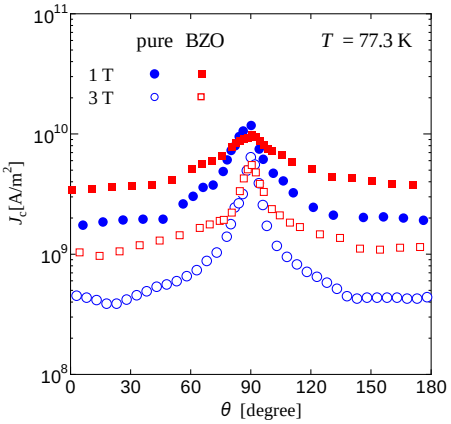

Fig. 4. Field angle anisotropy of critical current density in TFA-MOD processed (YGd)$Ba_2Cu_3O_{7-x}$ with and without $BaZrO_3$ nano-particles [23].

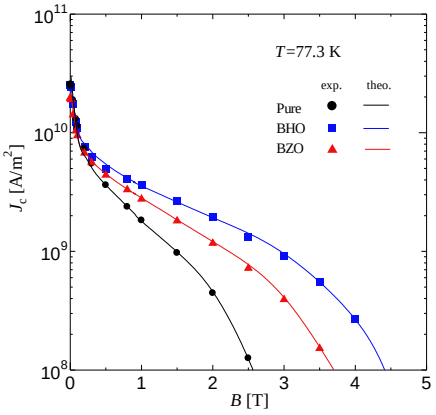

Fig. 5. Magnetic critical current density at 77.3 K in the magnetic field along the c -axis for $GdBa_2Cu_3O_{7-x}$ samples with $BaHfO_3$ and $BaZrO_3$ nano-rods [24]. The solid lines are theoretical predictions for each sample.

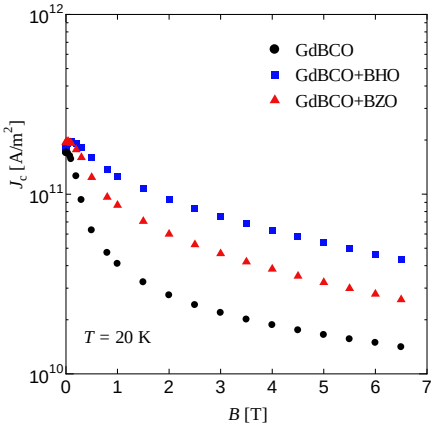

Fig. 6. Magnetic critical current density at 20 K in the magnetic field along the c -axis for $GdBa_2Cu_3O_{7-x}$ samples with $BaHfO_3$ and $BaZrO_3$ nano-rods.

logarithm of time. The apparent pinning potential is defined by [25]

$$U_0^* = k_B T \left[-\frac{\partial}{\partial(\log\ t)} \left(\frac{M}{M_0} \right) \right]^{-1} = \frac{k_B T}{S}, \quad (3)$$

where k_B is the Bolzmann constant, M is the magnetization, M_0 is the initial magnetization and S is the logarithmic relaxation rate. The results of U_0^* obtained by fitting a linear line to the observed M/M_0 vs. $\log\ t$ curve are shown in Fig. 7. The change in U_0^* by addition of nano-rods is not simple. However, it contributes to the enhancement of U_0^* or reduction in S at high magnetic fields that is required for high-field application. The improvement of the relaxation property for BHO nano-rods is pronounced.

2.4. Improvements by thick superconducting layer

The superconducting layer thickness plays an important role in the flux creep, since it influences the value of the pinning potential. The longitudinal flux bundle size is given by [26]

$$L = \left(\frac{B a_f}{2\pi \mu_0 J_{c0}} \right)^{1/2}, \quad (4)$$

where a_f is flux line spacing and J_{c0} is the virtual critical current density in the creep-free case. This length increases with increasing magnetic field and reaches the superconducting layer thickness at some normal magnetic field. Hence, the pinning becomes two-dimensional and the pinning potential takes a smaller value than a thicker superconducting tape at high fields, since the longitudinal flux bundle size is limited by the thickness. Figure 8 shows the variation in the apparent pinning potential with the superconducting layer thickness at 20 K in the magnetic field parallel to the c -axis for TFA-MOD processed (YGd)$Ba_2Cu_3O_{7-x}$ with BZO nano-particles. The added amount of BZO was 1 wt%. The specification of the specimens is given in Table 2. The magnetization critical current density of these specimens is shown in Fig. 9. The superconducting layer thickness of J_c is not simple and J_c in the thickest specimen #3 is lowest. Nevertheless the apparent pinning potential is largest at high fields in this sample. This can be attributed to the enhanced volume of flux bundle as expected theoretically. However, the apparent pinning potential of the thinnest specimen #1 takes a larger value than specimen #2. This point seems to be contradictory and will be discussed in section 3.4.

3. THEORETICAL APPROACH AND DISCUSSION

The role of the number of flux lines in the flux bundle, g^2, plays an important role in determination of the pinning potential in the theoretical analysis. It tends to strongly increase with increasing temperature and/or magnetic field as shown in Eq. (A5), whereas the variation in g_e^2, the g^2 value for the virtual perfect flux line lattice, is not appreciable. The statistical distribution of flux pinning strength was not assumed in the theoretical estimation of g^2 [27]. Hence, the theoretically predicted value of g^2 is sometimes larger than the value determined as a fitting parameter, although its dependence on temperature,

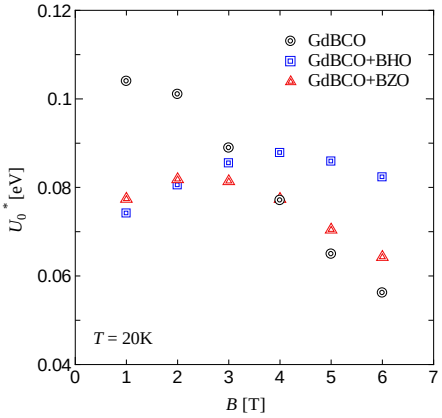

Fig. 7. Apparent pinning potential at 20 K in the magnetic field along the c-axis for $GdBa_2Cu_3O_{7-x}$ samples with $BaHfO_3$ and $BaZrO_3$ nano-rods.

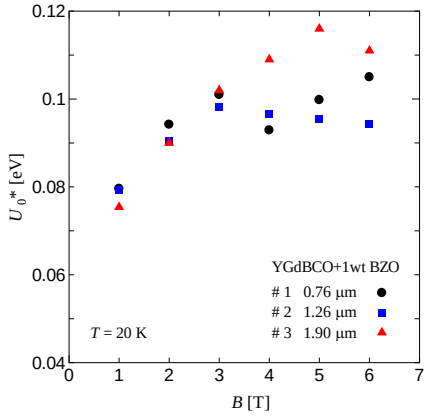

Fig. 8. Apparent pinning potential at 20 K in the magnetic field along the c-axis for $(YGd)Ba_2Cu_3O_{7-x}$ samples of different superconducting layer thicknesses with $BaZrO_3$ nano-rods.

magnetic field and superconducting layer thickness is similar [28]

Here we have another problem in the theoretical estimation of g^2 for a superconductor with different two kinds of pinning centers, such as natural and artificial pinning centers. In this case we assume an equivalent virtual pinning centers of a single kind as will be done in section 3.2. The suitability of this method was checked by comparing the creep-free current density with the theoretical estimate for the collective summation such as Eq. (1) in the low magnetic field region [24]. Hence, it can be expected that the value of g^2 can be estimated using Eq. (1) for J_{c0}.

In the following the experimental results are compared with the theoretical estimation for each aspect.

3.1. Field-angle anisotropy

Here we theoretically analyze some experimental results. The flat field-angle dependence shown in Fig. 2 is not treated, since it is not easy to take account of the distribution of growing angle shown in Fig. 3. On the other hand, the field angle anisotropy shown in Fig. 4 is theoretically analyzed. For simplicity we disregard the

TABLE II
SPECIFICATION OF TFA-MOD PROCESSED $(YGd)Ba_2Cu_3O_{7-x}$ SAMPLES.

Sample	Thickness d (μm)	T_c (K)
#1	0.76	89.5
#2	1.26	90.2
#3	1.90	90.0

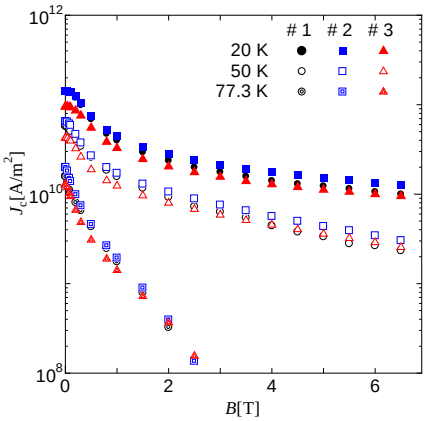

Fig. 9. Magnetic critical current density of $(YGd)Ba_2Cu_3O_{7-x}$ samples of different supercon- ducting layer thicknesses with $BaZrO_3$ nano-rods in the magnetic field along the c-axis.

effect of flux creep because we treat the pinning property at low magnetic fields. If we treat the pinning property at high fields, the theoretical analysis including the effect of flux creep is needed. The core interaction, i.e., the δT_c interaction of isotropic non-superconducting particles is simply assumed, since the strain induced around nano-particles produced by TFA-MOD method was found to be very much localized near the interfaces with the matrix [29]. For simplicity, therefore, the δl pinning by surrounding strained region is disregarded. It is expected that this assumption does not cause a large quantitative error, since the δT_c pinning that utilizes the maximum energy difference, i.e., the condensation energy, is strongest.

The anisotropic pinning force density by natural defects is assumed as [30]

$$F_{np}(B,\theta) = J_{nc}(\theta)B = J_c(0)B(\cos^2\theta + k^{-2}\sin^2\theta)^{-a}, \quad (5)$$

where $J_c(0)$ is the critical current density in the magnetic field along the c-axis and k is given by $J_c(\pi/2)/J_c(0)$ with $J_c(\pi/2)$ denoting the critical current density in the in-plane field. Although this assumption is similar to the result of anisotropic theoretical model of electron effective mass, we use k as a fitting parameter as well as a. The reason why we do not use the theoretical model is that it sometimes takes a value much smaller than the true anisotropy.

The nano-particle size D_g is about 20 nm and is larger than $2\xi_{ab}$ and $2\xi(\theta)$ at 77.3 K, where ξ_{ab} is the coherence length in the a-b plane and θ is an angle of the magnetic field from the c-axis. The pinning energy is given by the

product of the condensation energy density $B_c^2/2\mu_0$ and the interaction volume V, where B_c is the thermodynamic critical field. For simplicity it is assumed that nano-particles are cubic of effective size D_g^* with its four surfaces normal to the direction of the Lorentz force. Such a simplified theoretical treatment has been employed in the analysis of flux pinning [31]. Then, it is natural to assume the volume is the same between the spherical and cubic nano-particles: $(D_g^*/D_g)^3 = \pi/6$ with estimating $D_g^* = 16$ nm. The maximum interaction volume is given by $V_m = \pi\xi_{ab}\xi(\theta)D_g^{*}$ and the corresponding maximum pinning energy is $U_{pm} = (\pi/2\mu_0)\ B_c^2\xi_{ab}\xi(\theta)D_g^*$. Since the energy changes from this value to 0 when the vortex core goes out of the nano-particle during displacement by $2\xi(\theta)$, the elementary pinning force, i.e., the maximum variation rate of the pinning energy with displacement of the vortex core, is given by

$$f_p = \frac{U_{pm}}{2\xi(\theta)} = \frac{\pi B_c^2 \xi_{ab} D_g^*}{4\mu_0}. \quad (6)$$

It is found that the elementary pinning force is isotropic for nan-particles sufficiently larger than $2\xi_{ab}$. In the above the pinning interaction only by nano-particle is assumed and the effect of new defects created around nano-particles is neglected for simplicity, since the pinning force of such defects will be much smaller than that of nano-particle itself.

Since each nano-particle is sufficiently smaller than the vortex spacing, it does not interact with plural vortices. Flux pinning by nano-particles is strong enough to result in the linear summation. Hence, the pinning force density caused by nano-particles is expected to be given as

$$F_{ap} = J_{ac}B = \eta_e N_p f_p \quad (7)$$

in the magnetic field below the matching field B^*, where η_e is the pinning efficiency smaller than 1. Empirically we can assume as $\eta_e \cong 0.3$ [14, 19]. For simplicity we assume that the matching field is the characteristic field at which the vortex spacing is equal to the mean spacing of nano-particles. In the magnetic field above the matching field some vortices are not caught by nano-particles, and hence, J_c decreases with increasing field as

$$J_{ac} = \frac{\eta_e N_p f_p}{B}. \quad (8)$$

Below the matching field all the vortices are pinned by nano-particles and the critical current density takes a constant value, $\eta_e N_p f_p/B^*$. Taking account of the contribution of natural defects the overall critical current density is directly obtained from Eq. (1) as

$$J_c = (J_{nc}^2 + J_{ac}^2)^{1/2}, \quad (9)$$

where J_{nc} is the critical current density caused by natural pinning centers.

Here we compare the theoretical estimation and experimental results shown in Fig. 4 [30]. At first we assume $k^2 = 49$ and $a = 0.56$ in Eq. (5) so as to obtain a good agreement for TFA-MOD processed $GdBa_2Cu_3O_{7-x}$ sample with no nano-rods (see Fig. 10). From the relationship of $B_c(T) = B_c(0)[1-(T/T_c)]$ in the high field region with $B_c(0) = 2.0$ T [32] and $T_c = 90.0$ K we have $B_c(77.3\ \text{K}) = 0.28$ T. Since the mean spacing of nano-particles is about 60 nm, we estimate as $N_p = d_p^{-3} = 4.6\times10^{21}$ m^{-3}. The matching field that satisfies the condition $a_f = d_p$ is estimated as $B^* = 0.67$ T. This leads to the critical current density $J_{ac} = 3.6\times10^9$ Am^{-2} caused by nano-particles at 1 T. The predicted field angle dependence of the sample with nano-particles is shown by solid line in Fig. 11, where the value of k^2 is changed to 38 to take account of the reduction of J_c in the in-plane magnetic field by introduction of nano-particles. Thus, the field-angle dependence of the sample with nano-particles can be approximately described by the present theoretical treatment.

In the case of nano-rods, the critical current density only in the magnetic field around the c-axis is improved. Hence, it is desirable that the growth direction of nano-rods is widely distributed as shown in Fig. 3 to obtain an isotropic field angle dependence. In the case of nano-particles, on the other hand, the peak of critical current density remains around the in-plane field. To reduce the anisotropy it is recommended to introduce high density of nano-particles.

3.2. High field property

Here we discuss the high-field critical current density and irreversibility field quantitatively. For this purpose the flux creep and flow model in Appendix is necessary. The experimental results shown in Fig. 5 for the samples with nano-rods parallel to the c-axis are treated for example. It can be seen that the high-field property is dramatically improved. This improvement is partly attributed by the enhancement of the upper critical field as will be shown later. This makes the theoretical treatment for high field properties complicated, since the experimental result of non-doped sample with low B_{c2} cannot be simply substituted as a contribution of natural pinning centers. See [24] as to the theoretical analysis for low field property in which the effect of B_{c2} is not important. For simplicity we approximate the pinning property of the sample with nano-rods is one with equivalent pinning centers of a single kind. Its virtual critical current density in the creep-free case is assumed in the form [33]:

$$J_{c0}(B) = AB^{\gamma-1}\left(1-\frac{B}{B_{c2}}\right)^{\delta}, \quad (10)$$

where γ and δ are parameters for the field dependence. For superconductors with high Ginzburg-Landau parameter κ, it is empirically known as $\delta = 2$. In Eq. (10) A is a parameter representing the flux pinning strength. It is assumed that A is statistically distributed as Eq. (A7) in Appendix II. The parameters A_m, σ and γ are determined so as to get a good agreements with experimental results. Figure 13 shows an example of comparison for the E-J curve obtained from the magnetization relaxation measurements. The determined parameters are listed in Table 3. Good agreements with experimental results are obtained as shown in Fig. 5.

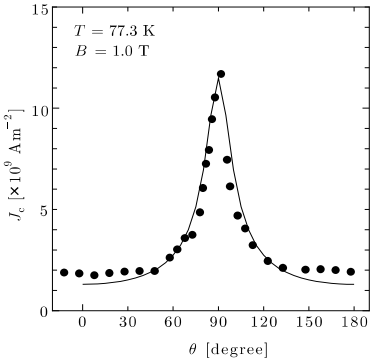

Fig. 10. Field angle anisotropy of critical current density in TFA-MOD processed pure (YGd)$Ba_2Cu_3O_{7-x}$ coated conductor. The solid line shows Eq. (5) with $k^2 = 49$ and $a = 0.56$ [30].

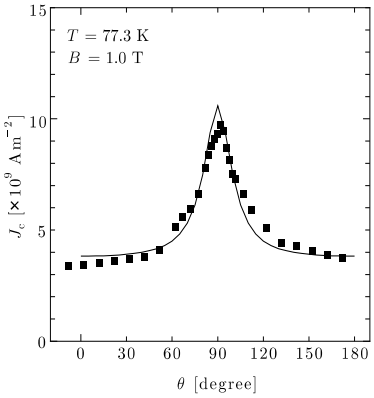

Fig. 11. Field angle anisotropy of critical current density in TFA-MOD processed (YGd)$Ba_2Cu_3O_{7-x}$ coated conductor with $BaZrO_3$ nano-particles. The solid line is theoretical prediction of Eq. (9) [30].

The upper critical field was measured for pure and doped samples with various amounts of BHO and BZO. The observed B_{c2} is plotted as a function of the area of the interface between nano-rods and the superconducting matrix in a unit volume in Fig. 13. The results show that B_{c2} increases linearly with increasing area of the interface. This indicates that the electron scattering at the interface reduces the coherence length through the reduction in the electron mean free path. It is not clear at this moment either of interface itself or heavily strained region around the nano-rods is dominant scattering centers. Anyhow the improvement of the high-field property is strongly supported by the enhancement of the upper critical field. The pinning characteristics expected in the virtual condition that only the flux pinning strength is improved are compared with the experiment in Fig. 14. The theoretical F_p value is determined from the calculated E-J relationship at the electric field criterion $E_c = 1 \times 10^{-9}$ V/m used in the magnetization measurements. It can be seen the improvement of the irreversibility field is clearly suppressed. Hence, the role of the upper critical field is important.

Even for similar nano-rods, the improvement of critical current density depends on the material of pinning centers. For example, the critical current density of sample with BHO is better as shown in Fig. 5. This is partly attributed to the stronger pinning force (compare the value of A_m shown in Table 3). The stronger pinning force comes from the larger number density of nano-rods (note that the diameter does not influence the pinning force by one nano-rod). In addition, the lattice mismatch at the interface was found to be smaller for the case of BHO [24]. It is also reported that the axial strain of the superconducting matrix around nano-rods is smaller for BHO whose Young's modulus is smaller [34]. For this reason the critical temperature is not seriously degraded, resulting in a larger B_c value in comparison with BZO. This point is important especially for application at 77.3 K. Another factor for the better high-field property is the higher B_{c2} shown in Fig. 13, which is caused by the larger interface area of BHO nano-rods with a smaller diameter.

3.3. Relaxation property

The relaxation property can also be analyzed using the flux creep and flow model. If the theoretical E-J curve shown in Fig. 12 is replotted as a magnetization relaxation with time, the apparent pinning potential is similarly obtained as in experiments. We treat the cases of BZO and BHO nano-rods in Fig. 7. The pinning parameters used for the analysis are given in Table 4 and the theoretical results are compared with experiments in Fig. 15. The lines show theoretical U_0^* values estimated from the theoretical magnetic relaxation calculated from the E-J relationship (E and J correspond to $\partial M/\partial t$ and M, respectively). Although the magnetic field dependence of U_0^* cannot be exactly reproduced, the improvement by addition of strong BHO nano-rods can be explained. The superior property in the sample with BHO nano-rods is attributed to the stronger pinning force (larger A_m value) and smaller distribution width represented by σ^2 value of the pinning force (see Table 4). The reason for the smaller distribution width is not clear.

TABLE Ⅲ
PINNING PARAMETERS OF PLD-PROCESSED $GdBa_2Cu_3O_{7-x}$ SUPERCONDUCTORS WITHOUT AND WITH NANO-RODS AT 77.3 K.

Sample	T_c [K]	B_{c2}(77.3 K) [T]	A_m [$\times 10^{10}$ Am^{-2}]	γ	σ^2 [$\times 10^{-2}$]	g^2			
						1.5 T	2.0 T	3.0 T	4.0 T
Pure	90.7	5.13	2.55	0.52	1.75	1.13	1.26	2.10	--
BHO	90.5	7.21	3.83	0.70	1.75	1.19	1.38	1.60	1.80
BZO	89.2	6.46	2.97	0.70	1.75	1.00	1.10	1.50	2.50

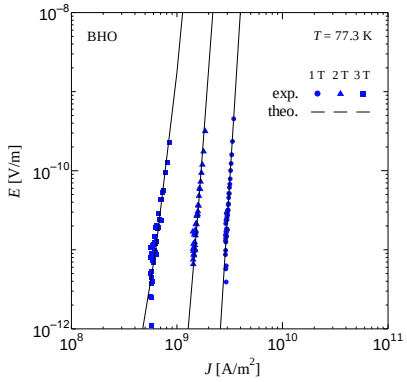

Fig. 12. E - J curves of the $GdBa_2Cu_3O_{7-x}$ coated conductor with $BaHfO_3$ nano-rods at 77.3 K in the magnetic field along the c -axis. Solid lines are theoretical predictions [24].

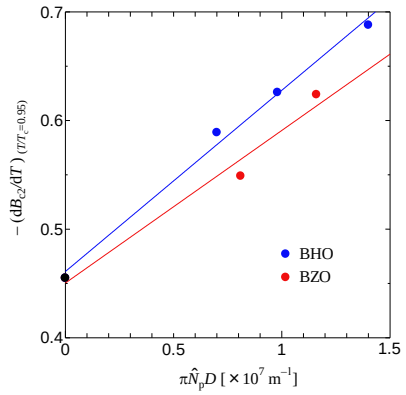

Fig. 13. Dependence of slope of B_{c2} vs. T curve at $T/T_c = 0.95$ for $GdBa_2Cu_3O_{7-x}$ coated conductors with $BaHfO_3$ and $BaZrO_3$ nano-rods on the area of interface between nano-rods and superconducting matrix in a unit volume [34].

3.4. Effect of superconducting layer thickness

Here we treat the effect of superconducting layer thickness on the irreversibility field determined by magnetization measurements. The irreversibility field observed using magnetization measurement for PLD processed pure $YBa_2Cu_3O_{7-x}$ coated conductors with different layer thicknesses is shown in Fig. 16 [35]. The specification of the samples is listed in Table 5. In spite of lower J_c the irreversibility field is higher in the thicker sample as predicted by the theory. The same results are obtained for CVD-processed $YBa_2Cu_3O_{7-x}$ with different layer thicknesses [28]. The apparent pinning potential U_0^* of the thickest sample #3 is the largest in the high field region as shown in Fig. 8 in spite of the lowest J_c value.

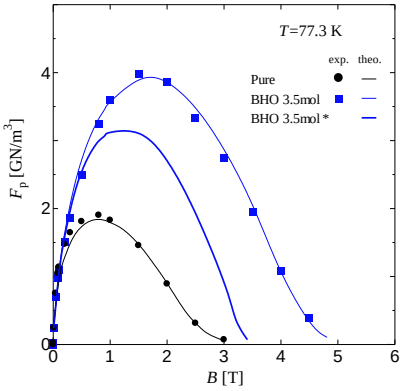

Fig. 14. Magnetic field dependence of pinning force density at 77. 3 K for $GdBa_2Cu_3O_{7-x}$ coated conductors with and without $BaHfO_3$ nano-rods. The middle solid line shows the theoretical F_p value under the condition that B_{c2} does not change by introduction of nano-rods [24].

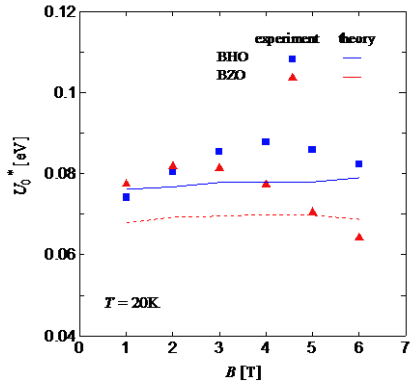

Fig. 15. Apparent pinning potential of $GdBa_2Cu_3O_{7-x}$ coated conductors with $BaZrO_3$ and $BaHfO_3$ nano-rods at 20 K shown in Fig. 7. Experimental results are compared with theoretical predictions.

This suggests the superiority of thicker superconductor as theoretically predicted. However, U_0^* value of the thinnest sample #1 is larger than that of #2. This seems to be contradictory.

The pinning correlation length L of #1 at 20 K and 5 T is estimated as 1.08 μm using Eq. (4) with J_c of about 1.2×10^{10} A/m² shown in Fig. 9, which is approximately used for J_{c0} because of low temperature region. The L value is longer than the thickness and hence, the pinning is in the two dimensional regime. Thus, the thermodynamic effect, i.e., the change in g^2, is expected to be pronounced as shown in Appendix. Since the longitudinal flux bundle size is limited by the film thickness d, the degradation in

TABLE Ⅳ
PINNING PARAMETERS OF PLD-PROCESSED $GdBa_2Cu_3O_{7-x}$ SUPERCONDUCTORS WITH $BaHfO_3$ AND $BaZrO_3$ NANO-RODS AT 20 K.

Sample	A_m [$\times 10^{11}$ Am^{-2}]	γ	σ^2 [$\times 10^{-2}$]	g^2
BHO	3.76	0.64	0.55	1
BZO	2.83	0.52	0.70	1

TABLE V
SPECIFICATION OF PLD-PROCESSED $YBa_2Cu_3O_{7-x}$ SAMPLES WITH DIFFERENT SUPERCONDUCTING LAYER THICKNESSES.

Sample	J_c in the self-field [$\times 10^{10}$ Am^{-2}]	d [μm]	T_c [K]
No. 1	2.60	0.50	88.4
No. 2	2.02	1.00	88.2
No. 3	1.53	1.50	88.4

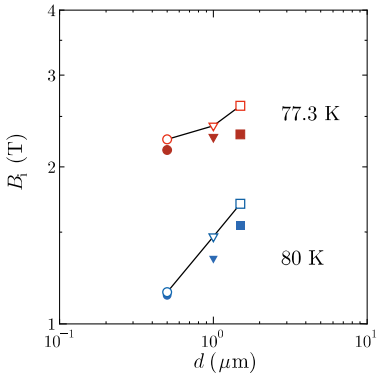

Fig. 16. Thickness dependence of irreversibility field along the c-axis of $YBa_2Cu_3O_{7-x}$ coated conductors at 77.3 and 80 K [36]. Open symbols show theoretical predictions and lines are guide for eye.

U_e is considered to enhance g^2 appreciably. This will be the reason why U_0^* in #1 becomes larger than that in #2. The pinning correlation lengths of #2 and #3 at the same condition are estimated as 0.98 μm and 1.18 μm, since J_c's are about 1.5×10^{10} A/m^2 and 1.0×10^{10} A/m^2, respectively. Hence, these lengths are smaller than the respective film thicknesses, resulting in the three-dimensional pinning regime. It means that the enhancement of g^2 does not occur and the trend between specimens #2 and #3 agrees the theoretical prediction. The important point is the J_c value. The self-field critical current density of #1 at 77.3 K is about 1.5×10^{10} A/m^2 and is not high. Now the fabrication technique is improved and the critical current density is much higher. Hence, the three-dimensional pinning regime will hold over a wide range of film thickness and the prediction on the thickness dependence on the relaxation property is expected to work.

As shown in the above the present theoretical approach is useful to estimate J_c in superconductors with APCs even under the appreciable effect of flux creep. It is even possible, therefore, to design J_c in the desired condition of temperature and magnetic field for specific application. That is, if the condition of application is fixed, the coherence length and the number density of flux lines are determined. We can select RE element and M in BMO to obtain a suitable size of pinning centers, which should be only slightly larger than the vortex core diameter. The matching condition under the aimed magnetic field is desired and the suitable amount of pinning centers to be added is determined. In this case it will be possible to estimate the enhanced upper critical field. It is also important to select the suitable thickness of the superconducting layer to reduce the effect of thermal activation. Then, the E-J characteristics can be calculated using the theoretical model with the assumed pinning parameters, and we can obtain J_c under the influence of flux creep using the electric field criterion suitable for the desired application. It is recommended to search the optimum condition of the size and number density of the pinning centers for the maximum J_c value.

4. CONCLUSION

In this paper the improvement of J_c properties in $REBa_2Cu_3O_{7-x}$ coated conductors with APCs is discussed. APCs are useful to improve not only J_c itself but also the field-angle anisotropy, high-field property and creep rate. The contribution of APCs to the overall J_c can be simply calculated with the linear summation model and the effect of thermal activation can be correctly estimated using the theoretical model of flux creep and flow. The superconducting layer thickness prays an important role in determination of the effect of flux creep: Thicker superconductor weakens the effect through a larger pinning potential, resulting in a higher irreversibility field and lower creep rate. The introduction of APCs is also beneficial from the viewpoint of improvement of the upper critical field, since the interfaces between APCs and superconducting matrix scatter electrons and reduce the coherence length. It is in principle possible to achieve the optimum pinning condition by properly designing APCs using the theoretical models of summation and flux creep and flow.

APPENDIX

The flux creep and flow model [12] is introduced here for the theoretical analysis of electromagnetic property under the flux creep in the magnetic field normal to the superconducting film. The key parameter that determines J_c under the flux creep is the pinning potential, U_0, which can be estimated using the virtual critical current density J_{c0} in the creep-free case. The dimensionality of flux pinning in the normal magnetic field is determined by the longitudinal flux bundle size L relative to the superconducting layer thickness d. In the three-dimensional pinning ($L < d$) the pinning potential is given by

$$U_0 = \frac{0.835 g^2 k_B J_{c0}^{1/2}}{(2\pi)^{3/2} B^{1/4}}, \quad \text{(A1)}$$

and in the two-dimensional pinning ($L > d$) the longitudinal flux bundle size is replaced by d and we have

$$U_0 = \frac{4.23 g^2 k_B J_{c0} d}{2\pi B^{1/2}}. \quad \text{(A2)}$$

In the above g^2 is the number of flux lines in the flux bundle, which is given by

$$g = \frac{R}{a_f} = \frac{1}{a_f}\left(\frac{C_{66}}{\alpha_L}\right)^{1/2} = \left(\frac{C_{66}}{2\pi J_{c0} B a_f}\right)^{1/2}, \quad \text{(A3)}$$

where C_{66} is the shear modulus of flux line lattice. In the virtual flux creep-free case the flux line lattice will be perfect and the shear modulus is theoretically given as [37]

$$C_{66}^0 = \frac{B_{c2} B}{8\mu_0 \kappa^2}\left(1 - \frac{B}{B_{c2}}\right)^2 \quad \text{(A4)}$$

Under the influence of thermal activation C_{66} is considered to be appreciably reduced from C_{66}^0; in the liquid state C_{66} is reduced to zero. It is not possible to theoretically determine the value of C_{66} in the practical situation. Then, it was proposed to determine C_{66} based on the principle of irreversible thermodynamics to maximize the practical J_c value under the flux creep [27]:

$$g^2 = g_e^2\left[\frac{5k_B T}{2U_e}\log\left(\frac{B a_f \nu_0}{E}\right)\right]^{4/3}. \quad \text{(A5)}$$

where ν_0 is the trail frequency, E is the electric field and g_e^2 is the value of g^2 for a perfect triangular flux line lattice given by

$$g_e^2 = \frac{B_{c2}}{16\pi\mu_0 a_f \kappa^2 J_{c0}}\left(1 - \frac{B}{B_{c2}}\right)^2 \quad \text{(A6)}$$

and U_e is the value of U_0 when g^2 is equal to g_e^2.

The magnetic field dependence of J_{c0} in a given temperature is assumed as Eq. (10). The statistical distribution of A in Eq. (10) is approximated as [12]

$$f(A) = K_A \exp\left[-\frac{(\log A - \log A_m)^2}{2\sigma^2}\right], \quad \text{(A7)}$$

where A_m is the most probable value of A, σ is a parameter representing a distribution width and K_A is a normalization constant. The E vs. J curve is calculated and the J_c value is determined with the electric field criterion. The detail of the analysis is described in [12].

REFERENCES

[1] J. L. MacManus-Driscoll, S. R. Foltyn, Q. X. Jia, H. Wang, A. Serquis, L. Civale, B. Maiorov, M. E. Hawley, M. P. Maley and D. E. Peterson, *Nature*, vol. 3, pp. 439, 2004.

[2] A. Goyal, S. Kang, K. J. Leonard, P. M. Martin, A. A. Gapud, M. Varela, M. Parathaman, A. O. Ijadoula, E. D. Specht, J. R. Thompson, D. K. Cristen, S. J. Pennycook and F. A. List, *Supercond. Sci. Technol.*, vol. 18, pp. 1533, 2005.

[3] M. Peurla, H. Huhtinen, M. A. Shakhov, K. Traito, Yu. P. Stepanov, M. Safonchik, P. Paturi, Y. Y. Tse, R. Palai and R. Laiho, *Phys. Rev. B*, vol. 75, pp. 184524, 2007.

[4] S. H. Wee, A. Goyal, J. Li, Y. L. Zuev, S. Cook and L. Heatherly, *Supercond. Sci. Technol.*, vol. 20, pp. 789, 2007.

[5] P. Mele, K. Matsumoto, T. Horide, A. Ichinose, M. Mukaida, Y. Yoshida, S. Horii and R. Kita, *Supercond. Sci. Technol.*, vol. 21, pp. 032002, 2008.

[6] H. Tobita, K. Notoh, K. Higashikawa, M. Inoue, T. Kiss, T. Kato, T. Hirayama, M. Yoshizumi, T. Izumi and Y. Shiohara, *Supercond. Sci. Technol.*, vol. 25, pp. 062002, 2012.

[7] S. Engel, T. Thersleff, R. Hühne, L. Schultz and B. Holzapfel, *Appl. Phys. Lett.*, vol. 90, pp. 102505, 2007.

[8] T. Aytug, M. Paranthaman, E. D. Specht, Y. Zhang, K. Kim, Y. L. Zuev, C. Cantoni, A. Goyal, D. K. Christen, V. A. Maroni, Y. Chen and V. Selvamanickam, *Supercond. Sci. Technol.*, vol. 23, pp. 014006, 2010.

[9] A. Palau, E. Bartolomé, A. Llordés, T. Puig and X. Obradors, *Supercond. Sci. Technol.*, vol. 24, pp. 125010, 2011.

[10] M. Miura, B. Maiorov, J. O. Willis, T. Kato, M. Sato, T. Izumi, Y. Shiohara and L. Civale, *Supercond. Sci. Technol.*, vol. 26, pp. 035008, 2013.

[11] See for example, V. Selvamanickam, M. H. Gharahcheshmeh, A. Xu, Y. Zhang and E. Galstyan, *Supercond. Sci. Technol.*, vol. 28, pp. 072002, 2015.

[12] M. Kiuchi, K. Noguchi, T. Matsushita, T. Kato, T. Hikata and K. Sato, *Physica C*, vol. 278, pp. 62, 1997.

[13] R. Labusch, *Crystal Lattice Defects*, vol. 1, pp. 1, 1969.

[14] E. J. Kramer, *J. Nucl. Mater.*, vol. 72, pp. 5, 1978.

[15] A. M. Campbell, *Phil. Mag. B*, vol. 37, pp. 149, 1978.

[16] A. I. Larkin and Yu. N. Ovchinnikov, *J. Low Temp. Phys.*, vol. 34, pp. 409, 1979.

[17] T. Matsushita and K. Yamafuji, *J. Phys. Soc. Jpn.*, vol. 48, pp. 1885, 1980.

[18] T. Matsushita, *Physica C*, vol. 243, pp. 312, 1995.

[19] T. Matsushita, N. Harada and K. Yamafuji, *Cryogenics*, vol. 29, pp. 328, 1989.

[20] T. Matsushita, *J. Phys. Soc. Jpn.*, vol. 84, pp. 034705, 2015.

[21] F. Matsutani, K. Himeki, M. Kiuchi, E. S. Otabe, T. Matsushita, S. Miyata, A. Ibi, Y. Yamada and Y. Shiokara, *Physica C*, vol. 469, pp. 1122, 2009.

[22] K. Kaneko, K. Furuya, K. Yamada, S. Sadayama, J. S. Barnard, P. A. Midgley, T. Kato, T. Hirayama, M. Kiuchi, T. Matsushita, A. Ibi, Y. Yamada, T. Izumi and Y. Shiohara, *J. Appl. Phys.*, vol. 108, pp. 063901, 2010.

[23] F. Matsutani, Y. Takahashi, M. Kiuchi, E. S. Otabe, T. Matsushita, M. Miura, T. Izumi and Y. Shiohara, *Physica C*, vol. 470, pp. 1411, 2010.

[24] T. Matsushita, H. Nagamizu, K. Tanabe, M. Kiuchi, E. S. Otabe, H. Tobita, M. Yoshizumi, T. Izumi, Y. Shiohara, D. Yokoe, T. Kato and T. Hirayama, *Supercond. Sci. Technol.*, vol.25, pp. 125003, 2012.

[25] T. Matsushita, "Flux Pinning in Superconductors," *Springer*, 2014, see Sec. 3.8.

[26] T. Matsushita, T. Fujiyoshi, K. Toko and K. Yamafuji, *Appl. Phys. Lett.*, vol. 56, pp. 2039, 1990.

[27] T. Matsushita, *Physica C*, vol. 217, pp. 461, 1993.

[28] K. Himeki, M. Kiuchi, E. S. Otabe, T. Matsushita, K. Shikimachi, T. Watanabe, N. Kashima, S. Nagaya, Y. Yamada and Y. Shiohara, *Physica C*, vol. 469, pp. 1457, 2009.

[29] M. Miura, B. Maiorov, M. Sato, M. Kanai, T. Kato, T. Kato, T. Izumi, S. Awaji, P. Mele, M. Kiuchi and T.Matsushita, *NPG Asia Materials*, vol. 9, pp. e444, 2017.

[30] T. Matsushita and M. Kiuchi, *TEION KOGAKU* (*J. Cryo. Super. Soc. Jpn.*), vol. 49, pp. 91, 2014 [in Japanese].

[31] A. M. Campbell, J. E. Evetts and D. Dew-Hughes, *Philos. Mag.*, vol. 18, pp. 313, 1968.

[32] T. Matsushita, M. Kiuchi, T. Haraguchi, T. Imada, K. Okumura, S. Okayasu, S. Uchida, J. Shimoyama and K. Kishio, *Supercon. Sci. Technol.*, vol. 19, pp. 200, 2006.

[33] A. M. Campbell and J. E. Evetts, *Adv. Phys.*, vol. 90, pp. 199, 1972 (see pp. 359).

[34] A. Tsuruta, Y. Yoshida, Y. Ichino, S. Sota, A. Ichinose, K. Matsumoto and S. Awaji, *TEION KOGAKU* (*J. Cryo. Super. Soc. Jpn.*), vol. 50, pp. 224, 2015 [in Japanese].

[35] T. Matsushita, K. Kimura, M. Kiuchi, E. S. Otabe , Y. Yamada and Y. Shiohara, *Supercond. Sci. Technol.*, vol. 20, pp. S189, 2007.

[36] T. Matsushita, H. Nagamizu, K. Tanabe, M. Kiuchi, E. S. Otabe, H. Tobita, M. Yoshimizu, T. Izumi, Y. Shiohara, D. Yokoe, T. Kato and T. Hirayama, *IEEE Trans. Appl. Supercond.*, vol. 23, pp. 8000304, 2013.

[37] E. H. Brandt, *Phys. Rev. B*, vol. 34, pp. 6514, 1986.